Shear-induced alignment in 3D-printed nitrile rubber-reinforced glass fiber composites

Guiyan Yang[1], Limin Qin[1], Mengru Li[1], Kangtai Ou[1], Jiang Fang[1], Qiang Fu[1, 2], Youyi Sun[1*]

1.School of materials science and technology, North University of China, Taiyuan 030051, P.R. China.

2.School of Civil and Environmental Engineering, University of Technology Sydney, Ultimo NSW 2007, Australia.

Abstract: Nitrile rubber composite with aligned glass fibers (GFs/NBR composites) were prepared by direct-ink-writing (DIW) technology for application in flexible thermal management of electronic equipment.The alignment and orientation (0^o, 45^o and 90^o) of glass fibers was precisely tuned by shear force field and 3D printing direction. Furthermore, the effect of print direction on the mechanical properties, thermal conductivity and heat dissipation performance were investigated. The tensile strength (1.78MPa) and thermal conductivity (1.2 $W\ m^{-1}\ K^{-1}$) of GFs/NBR composites with a 90^o orientation was improved to be 149.6% and 300% compared to the composites with disordered orientation, respectively. The temperature of LED device and computer' CPU covered with GFs/NBR composites with a 90^o orientation was reduced by *ca.* 8.1°C and 4.1°C, respectively. The study confirmed the formation of GFs/NBR composites with controlled alignment and orientation for various applications.

Keywords: Multifunctional composites; anisotropic particles; 3D printing; shear-thinning; thermal management.

Responding author: Fax: 86-351-3559669

E-mail address: syyi@pku.edu.cn (YY Sun)

1. Introduction

Electronic and mobile devices are undergoing a process of miniaturization, light weight and multi-functionalization [1]. The higher the degree of integration, the more internal heat is generated, which is the main reason for the reduced performance and shortened life cycle of electronic and mobile devices [2]. Therefore, the heat dissipation materials are highly demanded in order to improve reliability and the lifetime of electronic and mobile devices [3]. However, these thermally conductive fillers with high heat transfer performance are difficult to be directly acted as heat dissipation materials due to be poor adhesion, such as boron nitride (BN) [4-5], aluminum nitride (AlN) [6], alumina (Al_2O_3) [7], silicon carbide (SiC) [8] and silicon dioxide fiber (SiO_2) [9]. To overcome above problems, these thermally conductive fillers were generally doped into polymer matrix for application in heat dissipation materials [10-14]. It has been reported that heat transfer performance of composites can be easily improved by increasing content of thermally conductive fillers. However, the content of fillers in the composites is usually limited to below 50wt% due to poor compatibility between the matrix and fillers, leading to a decrease of mechanical properties. Recently, it is found that the heat transfer performance of composites can be effectively improved by tuning the alignment of anisotropic fillers [15-19]. Therefore, some methods have been developed to tune and control the alignment and orientation of anisotropic fillers, such as Mold casting, Stereolithigraphy Apparatus (SLA), Fused Deposition Modeling (FDM) and direct-ink-writing (DIW) technology[20]. Among these methods, direct-ink-writing (DIW) technology is the most promising process to tune and control the alignment of anisotropic fillers in the polymer composites due to be suitable for more materials, in which almost any material can be constructed to complex 3D shapes [21]. For example, Collino et al reported the preparation of SiC fibers/epoxy composites with aligned structure by acoustic-field-assisted DIW technology[22]. Naleway et al reported the preparation of nickel-coated carbon fibers/photopolymer resin composites with aligned structure by ultrasound-field-assisted DIW technology[23]. Lewis et al reported the preparation of SiC/C-filled epoxy composites with aligned structure by shear-field-assisted DIW technology[24-25]. Lewicki et al also reported the preparation of carbon fibers/epoxy composites with aligned structure by shear-field-assisted DIW technology[26]. Although the DIW technology has been used to prepare the polymer composite with aligned fibers, yet, the content of fibers in the composites is usually limited to below

30wt%. With higher contents of fibers, clogging of 3D printing nozzle becomes challenging.

Here, Nitrile rubber composite with aligned glass fibers were prepared by direct-ink-writing (DIW) technology for application in flexible thermal management of electronic equipment. A new shear-thinning gels with high content (more than 40wt%) of fibers was designed and prepared. Furthermore, the alignment and orientation of GF in NBR composites can be facilely and precisely controlled by shear force and printing direction of nozzle. The influence of printing direction on the mechanical properties, thermal conductivity and heat dissipation of the GFs/NBR composites were investigated. These results confirmed the foramtion aligned GFs/NBR composites with high heat dissipation performance for potential applications in sensors and flexible electronics

2. Experimental

2.1 Materials

Nitrile rubber latex (NBR, 43.5wt% of NBR content, FSDJ52) was supplied by Lao chemical Co., Ltd. Glass fibers (GFs, length of 300-600 μm, Diameter of 10μm, E type, strength of 2502MPa, modulus of 70.2GPa) were supplied by Hangzhou Corker composite material Co., Ltd. Oleicacid (OA) and triethanolamine (TEOA) were purchased from Tianjin Kaitong Chemical Reagent Co., Ltd. Fumed silica (SiO_2) were purchased from Aladdin.

2.2 Preparation of graphene nanosheets

Graphene was prepared by water-exfoliated method. First, 30g $KMnO_4$ was added into 180mL concentrated sulfuric acid in the ice bath. When the mixture cooled down, the ice bath was removed and 30 g natural graphite was added. The system was stirred under ambient conditions for 1 hour. Then, 30 g Na_2CO_3 was added into above mixture under mechanical stirring. Second, 420 mL H_3PO_4 was added into above mixed system and mechanically stirred for another 5 hours. Thereafter, the products were washed and filtered, forming bubbling expansion graphite. In a control experiment, graphite intercalation compounds (GICs) were also prepared according previous literature without adding Na_2CO_3 and H_3PO_4. Third, 30 g BEG or GIC was added into 750 mL NaOH solution (pH=14). The mixture was sheared for 2 hours at 15,000 rpm using an FA 40 high shear dispersing emulsifier (Fluko) with a working tool. Thereafter, the BEG-based mixture was added to sand-milling machine for 12 hours.

2.3 DIW 3D printing process of polymer composites

GF/G/NBR composite with aligned structure was prepared by the DIW 3D printing technology as shown in Scheme 1. The shear-thinning gels (inks) were prepared by the multiple steps, in which the formula was concluded in Table 1. 20.0g Nitrile latex and 1.0g triethanolamine were firstly mixed under mechanical stirring. The process avoided the demulsification of NBR latex solution, resulting in agglomeration and precipitation of NBR latex particle. Then 0.15g graphene and 0.5g fumed silica were added to above mixing solution under mechanical stirring with 600rpm for 3.0min. Then, 15.0g glass fibers were added to above mixing solution under mechanical stirring with 600rpm for 5.0min. Finally, 2.0g oleic acid was added to above mixing solution under mechanical stirring with 600rpm for 2.0min. When the mechanical stirring was stopped, the mixing solution immediately changed to gel. It can effectively avoid the agglomeration and precipitation of glass fibers. The 3D composite objects were then fabricated by 3D printing the shear-thinning gels at a speed of 10mm/s. The printing process was carried out on desktop printer (Scheme 1A) with a new rotary-screw head with 0.6mm nozzle (Scheme 1B). Geometries were designed by computer aided design (CAD) files. The printed composites were cured at 145.0^{o}C for 25.0min. In a comparison, the object without GF was prepared by 3D printing inks. The disordered composite was prepared by molding method, in which the composition is same with formula of inks materials (in Table 1). The inks materials were directly added to mold and dried at room temperature for 12h. Finally, the sample was further cured at 145.0^{o}C for 25.0min.

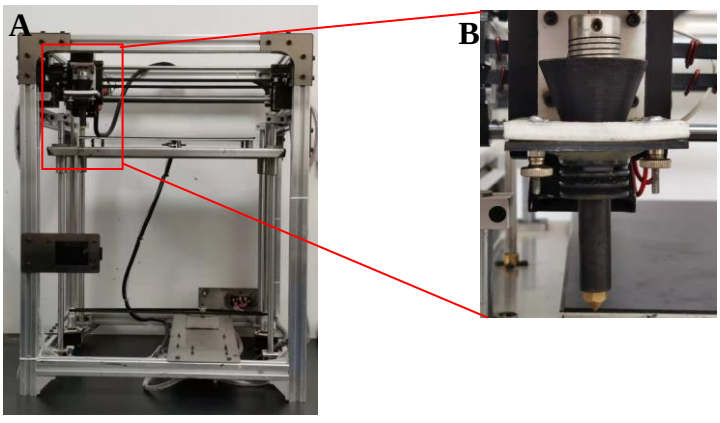

Scheme 1. Optical photo of (A) present 3D printing setup and (B) nozzle based on screw extrusion.

Table 1. formula of inks materials.

Ink composition	Nitrile rubber latex	Glass fibers	Oleic acid	Triethanolamine	Fumed silica	Graphene
Quality (g)	20.0	15.0	2.0	1.0	0.25	0.15
Wight%	52.1%	39.1%	5.2%	2.6%	0.65%	0.39%
Volume%	50.3%	42.7%	2.1%	1.1%	2.2%	1.6%

2.4 Characterization

Fourier transform infrared (FT-IR) spectroscopy of samples was measured by FT-IR analyzer (FTIR-8400s) at 4000~400cm^{-1}.

The shear-thinning effect was characterized by a rheometer (MCR-302, Anton Paar, Austria) with a 20.0mm flat plate device (1.0mm gap). Specifically, the steady-state mode with a shear rate of 0.01-1000 s^{-1} was used for viscosity measurement. The storage modulus (G') and loss modulus (G") were measured at anoscillation mode with an angular frequency of 10 rad/s and a shear stress ranging from 0 to1000 Pa.

A ZEISS metallurgical microscope was used to photograph the Orientation characteristics of the glass fibers in the extruded filaments.

The micro-structure of samples were characterized by Scanning electron microscope (SEM, SU-8010) at 5.0kV acceleration voltage. Before characterizations, all the samples were immersed in liquid nitrogen to form brittle sample, which could be easily fractured by hand.

The mechanical properties of rectangular specimens (60mm×6mm×3mm) were measured by a multifunctional testing machine (AI-7000-SGD) at room temperature. The DLR-3 thermal conductivity meter was used to measure the thermal conductivity of the film sample (20mm×3mm).

An anisotropic film (30mm×12mm×2mm) was prepared and placed on a constant temperature heating table at 65.0^{o}C to record the temperature change of the film with infrared thermal imaging.

The temperature distribution images of the samples were taken by an infrared imaging device (FLUKE, FLIR Systems, Inc., USA).

The heat dissipation was characterized as shown in following. A block (12mm×5mm×4mm) acted as the base of the LED chip, and surface temperature of the chip was detected by an infrared thermal imager. According to the position of the

electronic components in the computer chipboard, a box was 3D printed and covered on the computer' chip, in which the surface temperature of the chip was detected by an infrared thermal imager.

3. Results and discussion

With the rapid development of flexible and wearable electronic and mobile devices, flexible heat dissipation materials are highly demanded for application in packaging or supporting materials. In this work, flexible heat dissipation materials with controlled alignment and orientation of thermally conductive fillers are fabricated *via* a 3D shear-thinning process (Fig.1). Under the action of the high-speed shear screw, the disordered GFs/NBR ink becomes fluid by shear thinning. which can easily flow out from the small nozzle. At the same time, GFs align and orient in the direction of fluid flow by the shear-induced method[27]. Moreover, the GFs/NBR fluids can immediately restore high viscoelasticity, forming filaments. As a result, the aligned and oriented GFs can be fixed in the filaments as shown in Fig.1A. And then the filaments were progressive deposition to form basic units to produce 3D structures.The orientation of GFs in GFs/NBR composites can be easily controlled by adjusting the printing direction of the nozzle (Fig.1B). Here, three composites with different orientations of GFs (0°, 45° and 90°) were designed and fabricated. To further demonstrate the good printability of present ink systems,a series of printing objects based on GFs/NBR composites were fabricated by DIW technology as shown in Fig.1C. The 2D structure (leaf, a&b) and 3D structure (octopuses, c&d) were printed using the GFs/NBR ink. The shape and size of the printed structures were the same as the CAD model, indicating that these inks had good structural fidelity and high resolution.

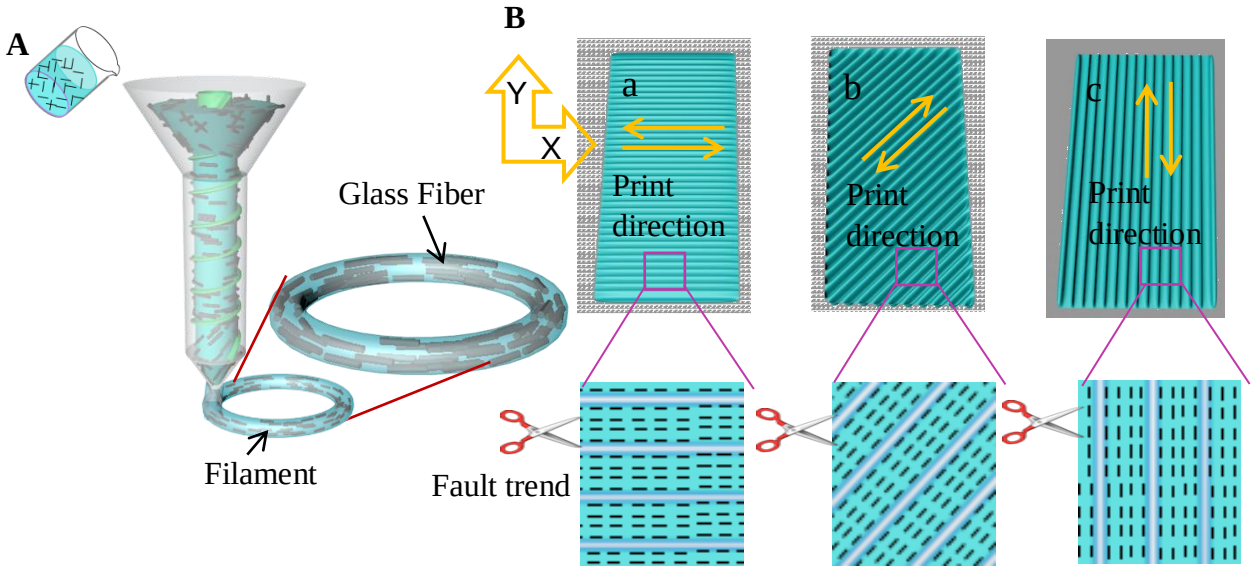

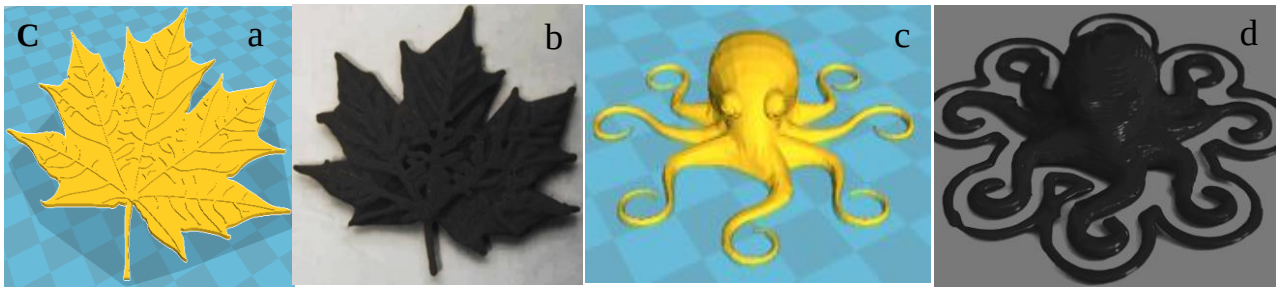

Fig.1. (A) Schematic diagram of the precise control of alignment and orientation of GFs in polymer composites via DIW 3D printing. (B) Schematic diagram of GFs/NBR composites with tunable aligned and orientation structures: (a) 0 °, (b) 45 °, and (c) 90°. (C) The CAD models and printed objects with various geometries, (a-b) the leaf and (c-d) the octopuses.

The design and preparation of shear-thinning inks were key role to the DIW 3D printing technology. Here, a shear-thinning ink based on supramolecular interaction between oleic acid (OA) and triethanolamine (TEOA) was developed to expand the types of printing materials (Fig.2A). As shown in Fig.2B, the absorption peaks at 1024.0cm^{-1} and 882.0cm^{-1} were observed, corresponding to vibration of C-N and C-H of TEOA, respectively. The absorption peaks at 2922.0cm^{-1}, 2850.0cm^{-1} and 1706.0 cm^{-1} were assigned to the vibration of C-H and C-O groups of OA, respectively. Meanwhile, these characteristic peaks of OA and TEOA were both observed in the IR spectrum of OA/TEOA hydrogel. In a comparison, the absorption peaks (1024.0cm^{-1} and 1706.0cm^{-1}) of OA/TEOA hydrogel significantly decreased comparing to single OA and TEOA. This result indicated the formation of the supramolecular interaction between C-O of OA and C-N of TEOA. It was interesting that after introduction of NBR latex, GFs and graphene (G), it still showed a stable gel for NBR/GFs/G/OA/TEOA composite (inset of Fig.2C). The rheological behaviors of the composite gel were characterized to evaluate its DIW printability as shown in Fig.2C-D. It was found that the the OA/TEOA gel and the composite gel exhibited a viscosity (η) of *ca.* 1×10^4 mPa•s and 2×10^5 mPa•s at low shear rate of ~0.01 s^{-1}, respectively (Fig.2C). When the shear rate increased from 0.01 to 1,000 s^{-1}, the η of the two gels both dramatically decreased to smaller than 10^2 mPa•s, indicating good shear-thinning effect. Fig.2D shows the G′ and G″ of these two samples as a function of shearing stress. It was found that the G′ of these two samples were both significantly higher than the G″. In addition, we observed a high shear yield stress (τ_y) of 80.0 Pa. These results indicated the formation of gel with high stiffness, which was

the key role for high shape fidelity of the printed 3D structures. Furthermore, these results also suggested that the incorporation of polymers or inorganic fillers had an ignorable effect on the rheological behavior of OA/TTA gel, making it suitable for DIW 3D printing. Compared to conventional DIW method, the present DIW approach shows several advantages, such as a more versatile 3D printing process for various materials, and a higher content of anisotropic particles in composites.

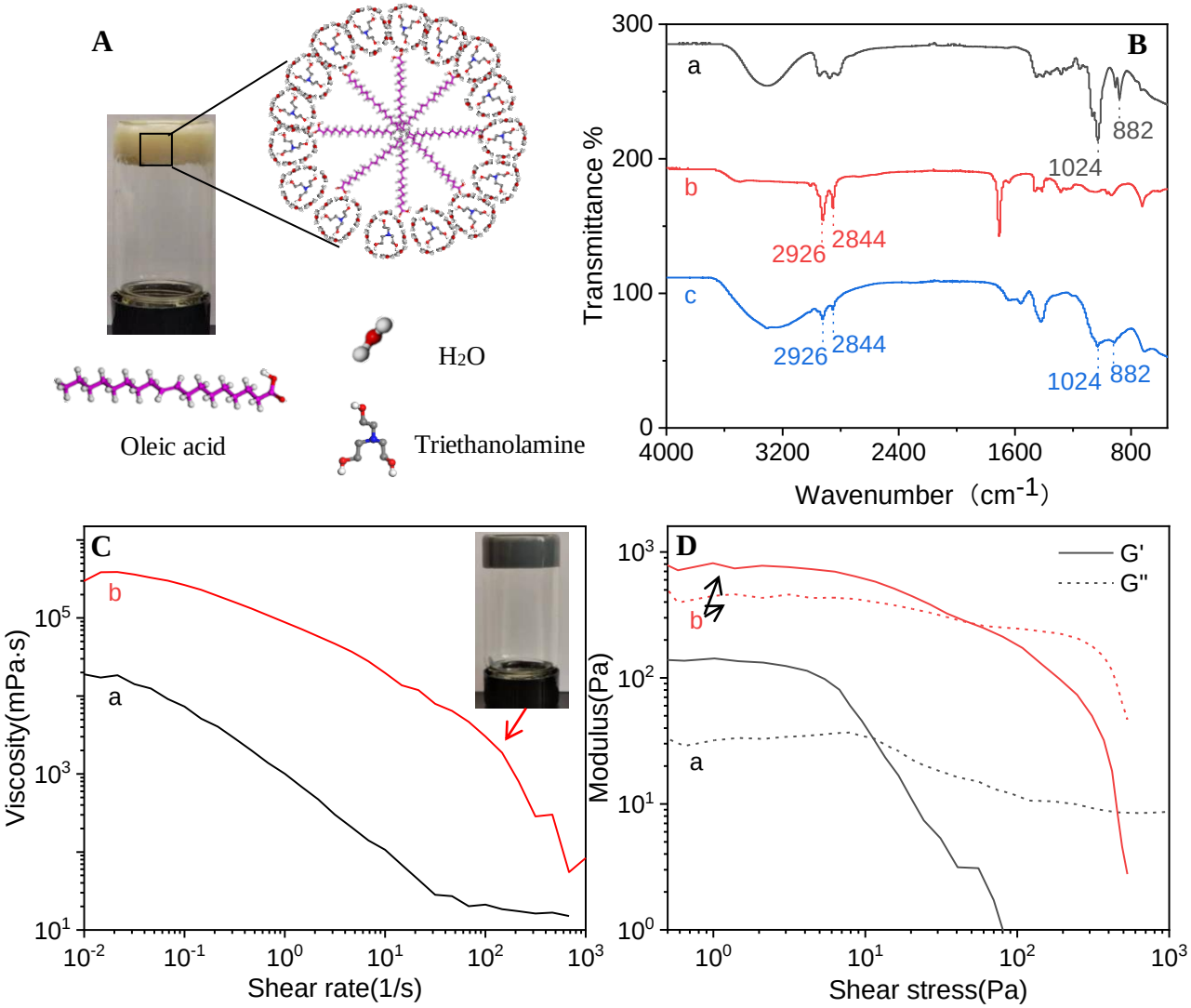

Fig.2. (A) Schematic diagram of the structure of OA/TEOA gel. (B) IR spectra of (a) TEOA, (b) OA and (c) OA/TEOA gel. (C) Viscosity *vs.* shear rate and (D) modulus *vs.* shear stress curves of (a) OA/TEOA gel and (b) OA/TEOA/NBR/GF/G composite printing ink. The inset of Fig.2C is the optical photo of OA/TEOA/NBR/GF/G composite printing ink.

The effect of OA/TTA mass ratio on the shear-induced alignment of GFs was also investigated. Fig.3A and 3B shows the rheological behaviors of the composite gel with various OA/TTA mass ratios. The composite gel with higher OA/TTA mass ratio

obviously showed larger higher viscosity and modulus. The result may be attributed to the more cross-linking point between OA and TTA as shown in the inset in Fig.3A. The micro-structure of GFs/NBR composite gels with various OA/TTA mass ratios was also characterized and compared during 3D printing process by the optical micro-photographs as shown in Fig.3C-D. It was found that the GFs were orderly orientation and alignment in the composite gel at high OA/TTA mass ratio (3:1). Contrarily, the GFs were disorderly distribution in the composite at low OA/TTA mass ratio (3:2). These results confirm the shear-induced alignment of GFs during 3D printing process, which also depends on the OA/TTA mass ratio. The result was attributed to that the composite gel with high OA/TTA mass ratio possessed high modulus. As well-known, the aligned GFs can be easily fixed in an composite gel with high modulus. Therefore, the modulus of DIW printing inks should be considered for the shear-induced alignment.

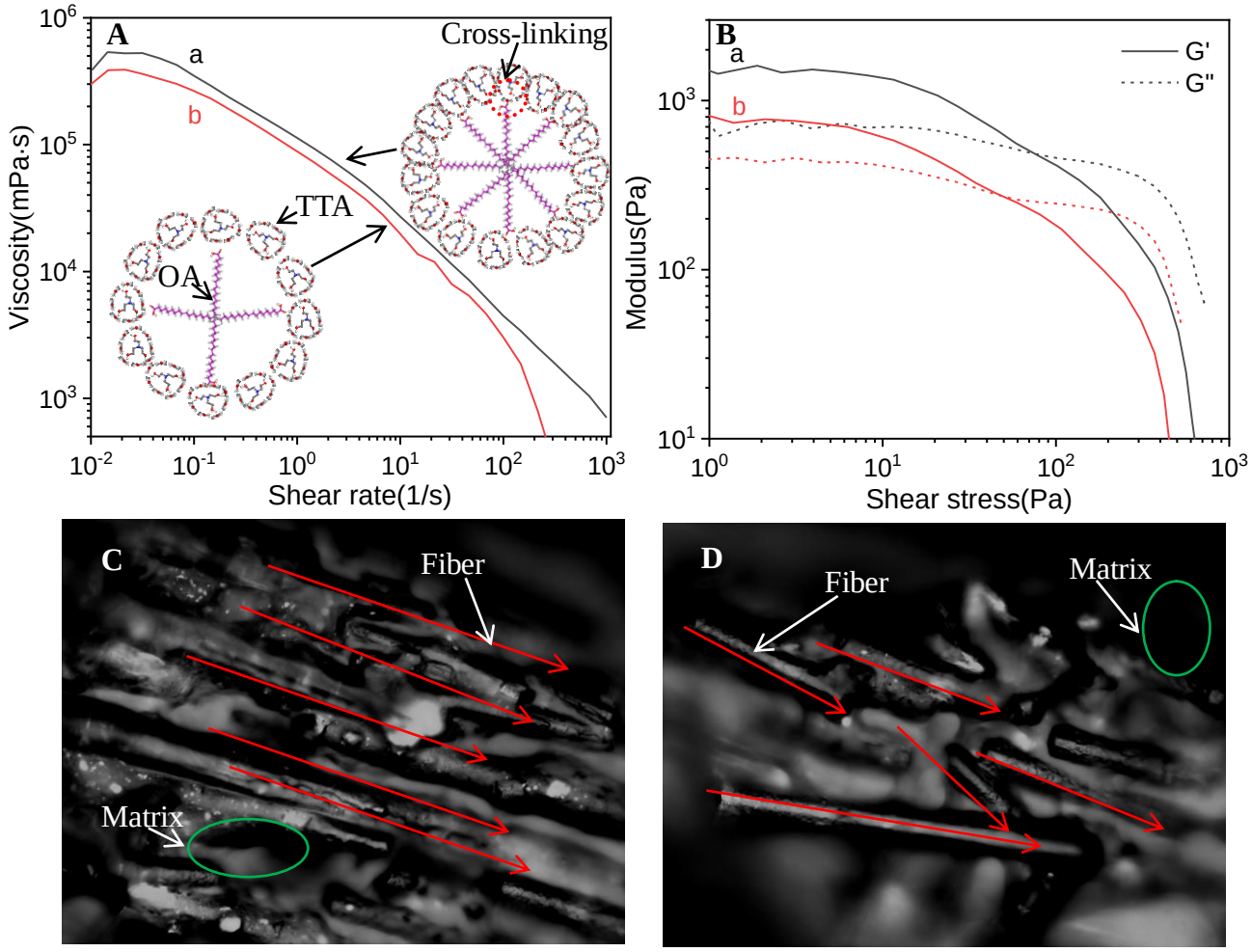

Fig.3. The curves of (A) viscosity *vs.* shear rate and (B) modulus *vs.* shear stress of composite gel with various OA/TTA mass ratios of (a) 3:1 and (b) 3:2. The optical

micro-photographs of extruded filaments based on composite gel with various OA/TTA mass ratios of (C) 3:1 and (D) 3:2. The insets in Fig. 3A are the schematic structure of OA/TEOA in composite gels with various mass ratios.

The micro-structure of the composites prepared by different 3D printing directions was characterized and compared by the SEM images (Fig. 4A-F). There presented a lot of closed fibers on the surface for all samples due to be high dopping content of GFs. Furthermore, these fibers were clearly ordered in orientation and arrangement, and few disordered fibers were observed as shown in Fig.4A-C. The result was difficult to be observed in previous works [28-31], in which some disordered fibers were always observed. In addition, it was found that it clearly showed different orientations (0^o, 45^o and 90^o) of GFs for the composites prepared by different 3D printing directions. Fig.4D-F shows the fractured surface SEM images of composites prepared by different 3D printing directions (0^o, 45^o and 90^o), respectively. The orientation of the GFs was parallel to the fractured surface for composites prepared by the 3D printing direction of 0^o. In contrast, the orientation of the GFs was perpendicular to the fractured surface of the other two composites prepared by the printing direction (45^o and 90^o). Furthermore, we found that the 3D printing composites had very few pores due to the high solid content of the present shear-shining ink. The micro-structure of the composites prepared by different 3D printing directions was further characterized and compared by the optical microscopes as shown in Fig.4H-J. The white and black picture represents the GFs and NBR matrix, respectively. It clearly showed that the GFs were well dispersed in NBR matrix. In addition, the orientation and alignment of fillers was consistent with printing direction in a large scale. In all, the GFs/NBR composites with ordered orientation and alignment of GFs were prepared by DIW 3D printing method, in which the orientation of fillers could be easily and precisely adjusted by the printing direction of nozzle.

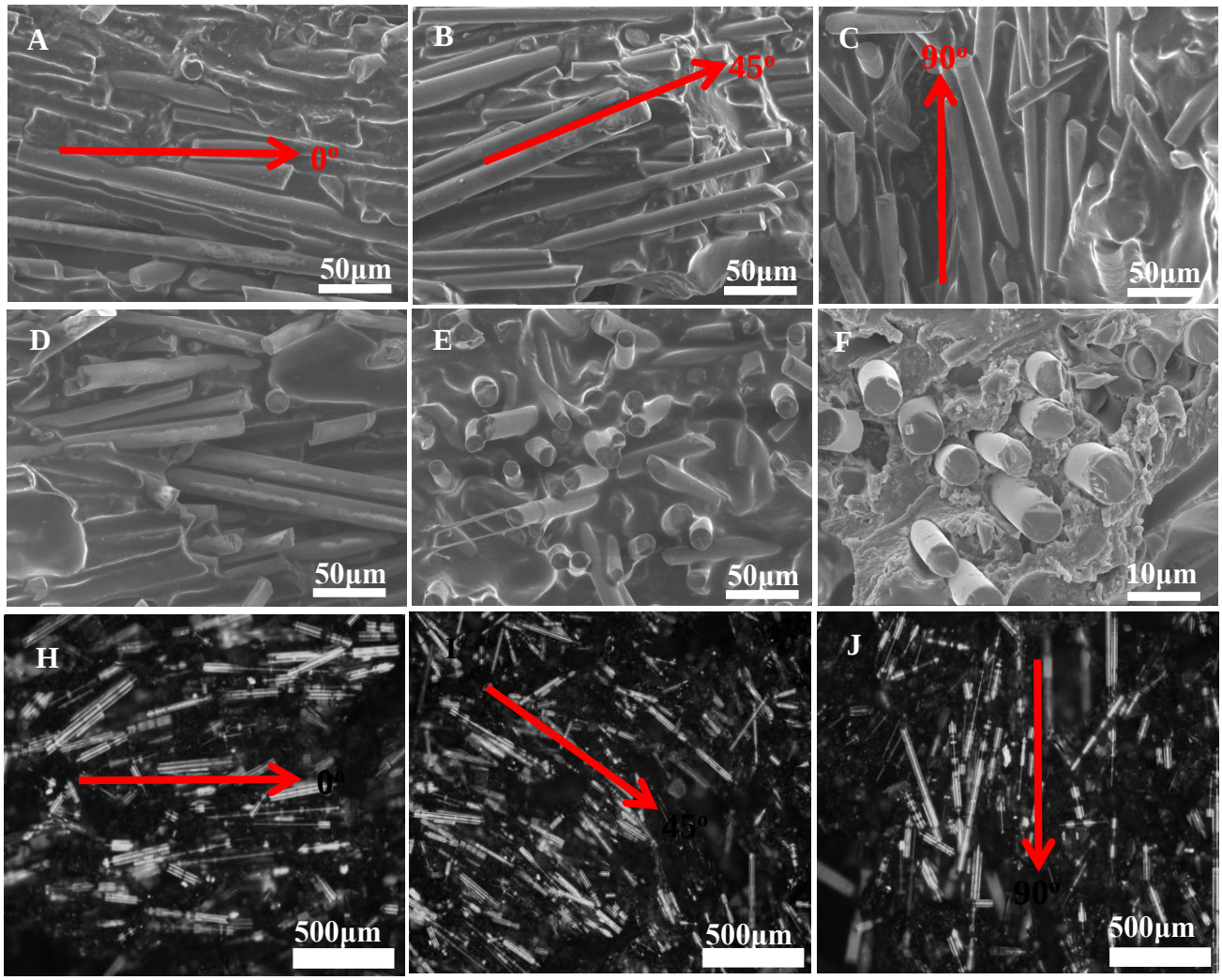

Fig. 4. SEM images of GFs/NBR composites with different printing directions of (A) 0°, (B)45° and (C)90°. SEM images of the fractured composite samples with different alignment and orientation: (D)0°, (E)45° and (F)90°. Optical microscopes of GFs/NBR composites with different printing directions of (H)0°, (I)45° and (J)90°.

Fig.5A shows the stress-strain curves of the composites with different printing directions (0°, 45° and 90°). It was found that the stress of all samples increased rapidly with the increase of strain in the first stage, and then increased moderately in the second stage. The rapid increase of stress was mainly attributed to the strong interaction between GFs and the NBR matrix, while the moderate increase was attributed to the weak interaction between the NBR chains. In a control experiment, the composite without GFs showed a pseudo-linear growth until fractured, indicating the weak interaction between NBR chains. In addition, all 3D printing composites with GFs exhibited higher tensile strength and smaller elongation at break compared with composite without GFs. The enhanced tensile strength was attributed to

reinforcing effect of GFs, which could significantly improve tensile strength of polymer composites[32]. The small elongation at break was due to the interface failure (poor compatibility) between the GFs and the NBR matrix. Furthermore, it was found that the mechanical properties of the composites also strongly depended on the printing directions. The composites with printing direction of 0^o and 90^o showed the lowest and the highest tensile strength, respectively (Fig.5B). The result was attributed to different orientations of GFs in NBR, resulting from different printing directions. When the tensile direction is parallel to the orientation of GFs (90^o), the deformation resistance of the composites comes from the GFs. the NBR matrix and the interaction between them, resulting in high tensile strength. In contrast, when the tensile direction is perpendicular to the orientation of GFs (0^o), the deformation resistance mainly comes from the NBR matrix and the interaction between matrix and fillers, leading to low tensile strength. The stress-strain curves of 3D printing composites (90^o) were further characterized as function of parallel and perpendicular tensile force as shown in Fig.5C, and the tensile strength and elongation data were summarized in Fig.5D. In the parallel direction, $\sigma_{a\parallel}$ and $\varepsilon_{a\parallel}$ of composites were 1.85±0.1MPa and 210.3±7.4%, while in the perpendicular direction, $\sigma_{b\perp}$ and $\varepsilon_{b\perp}$ of composites were 0.75±0.1MPa and 175.2±7.0%, respectively. The anisotropic mechanical properties of composite with printing direction of 90^o further indicated the orderly arrangement of GFs in NBR matrix. These results again confirmed the successful preparation of polymer composites with controlled orientation, which exhibited excellent anisotropic mechanical properties.

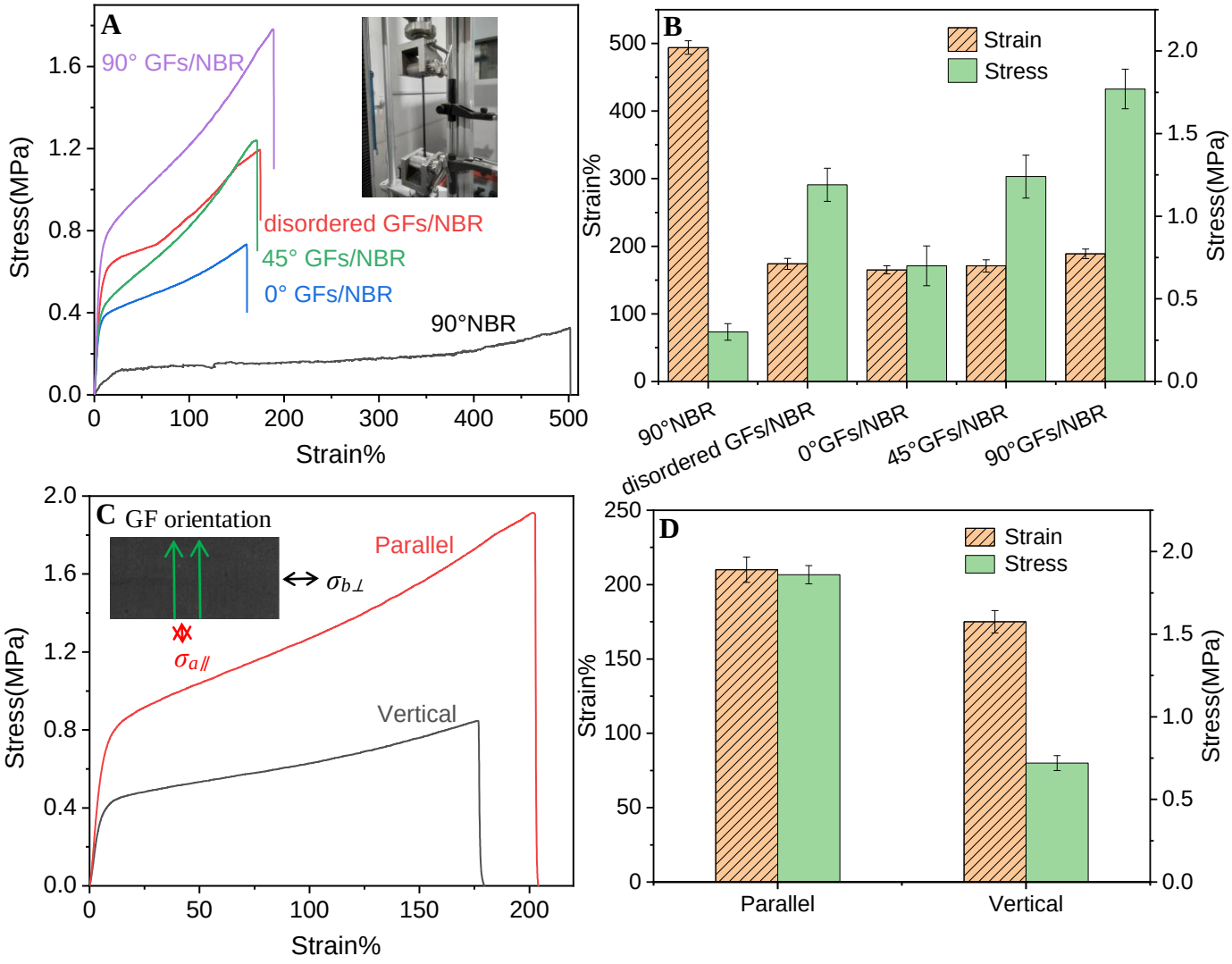

Fig.5. (A)Stress-strain curves and (B)Tensile strength and elongation of (a) composite without GFs, (b) disordered composite with GFs and composite with GFs prepared by different printing directions of (c) 0°, (d) 45° and (e) 90°. (C)Stress-strain curves and (D)Tensile strength and elongation of composite with GFs (90°) under along (a) parallel and (b) perpendicular to the printing direction.

The thermal conductivity of the composites with different printing directions (0°, 45° and 90°) was also characterized and compared as shown in Fig.6A. The composite without GFs and the disordered composite with GFs showed similar thermal conductivity of *ca.* 0.4W $m^{-1} K^{-1}$. The result was due to that it did not form thermally conductive network for the two composites. In a comparison, the thermal conductivity of the composites with different 3D printing directions of 0°, 45° and 90° were all improved to 0.9 W $m^{-1} K^{-1}$, 1.1 W $m^{-1} K^{-1}$ and 1.2W $m^{-1} K^{-1}$, respectively. The

enhanced thermal conductivity was attributed to the formation of thermally conductive network, resulting from the ordered orientation and alignment of GFs in NBR matrix[17-19]. The thermal transfer performance of composites with different printing directions was also characterized and compared by infrared thermal imaging (Fig.6B). The thermal transfer direction of the composites was almost consistent with the printing directions. The heat generally transfers along the thermal conductive network[16]. These results further confirmed the formation of thermal conductive network, effectively improving the thermal transfer performance. The surface temperatures of the composites as a function of heating time were recorded in Fig.6C. After placed on a hotplate for 175s, average surface temperature of 3D printing composites with different printing directions of 0º, 45º and 90º was *ca.* 58.5ºC, 61.0ºC and 64.5ºC, respectively. In a comparison, the average surface temperature of the disordered composite was only 36.5ºC. This result further indicated that the composites with ordered orientation of GFs were easier heat transfer comparing to disordered composite. The enhanced thermal transfer performance of composites with ordered structure was analyzed as shown in Fig.6D. When the direction of heat transfer is parallel to the orientation of GFs, the heat is easily transferred between GFs. On the contrary, when the heat transfer direction is perpendicular to the orientation of GFs, it is difficult to transfer heat due to the heat transfer resistance between GFs and the NBR matrix. In all, these results reveal that the 3D printing composites with ordered orientation have good heat transfer performance for potential application in heat dissipation and diffusion.

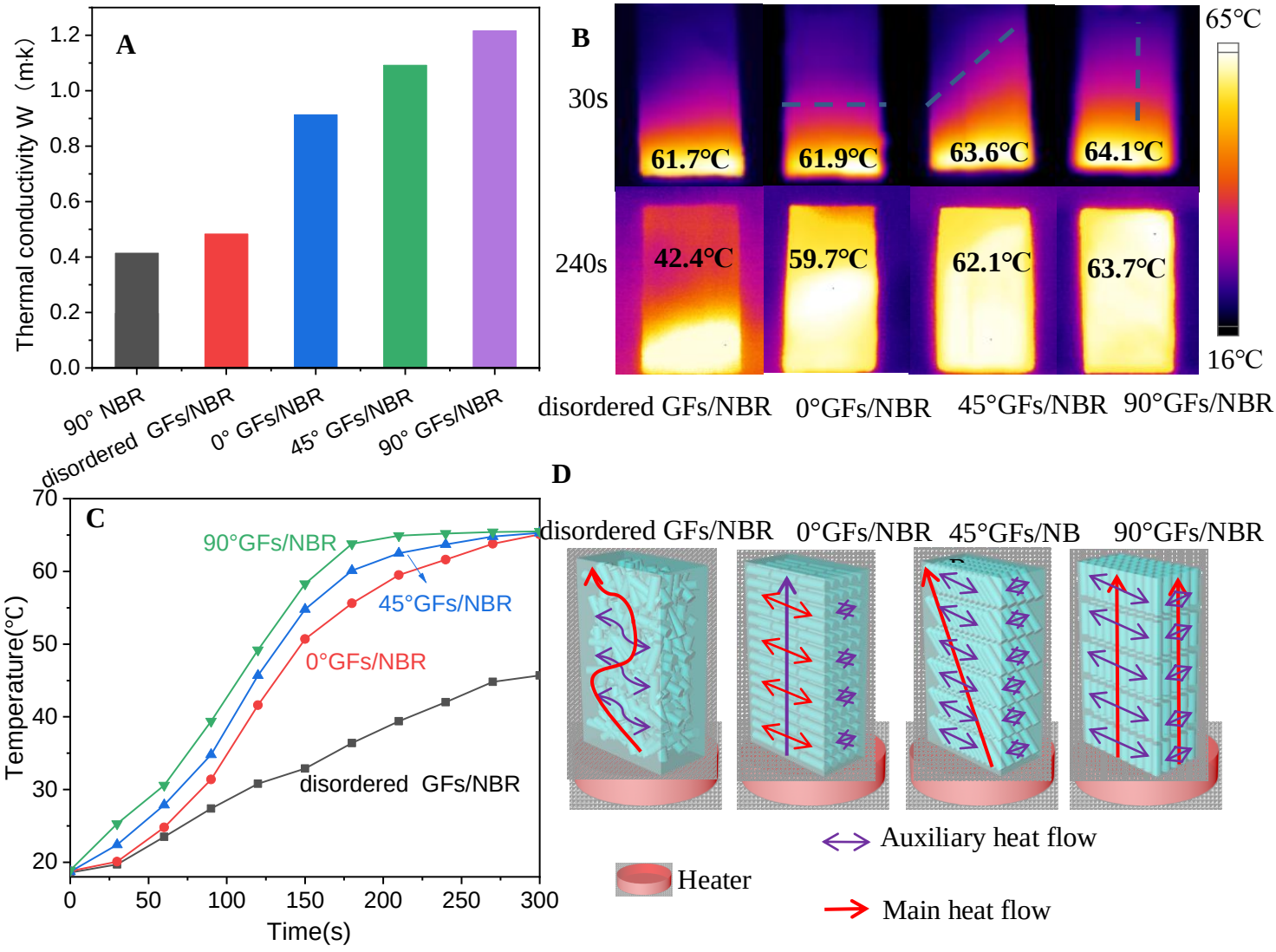

Fig.6. (A)Thermal conductivity of (a) composite without GFs, (b) disordered composite with GFs and composites with different different printing directions of (c) 0º, (d) 45º and (e) 90º. (B) Infrared thermography of heat transfer, (C) temperature *vs.* time curves and (D) schematic diagram of heat transfer mechanism of (a) disordered composite and composites different printing directions of (b) 0º, (c) 45º and (d) 90º.

Previous studies have reported that when the temperature of electronic components rises by 2.0℃, the reliability of electronic components decreased by 10%. For example, the lifetime of electronic components at 50.0℃ is only 1/6 of that at 25.0℃. Therefore, speeding up the heat dissipation of electronic components is very important. However, due to the inevitable gap between the surface of the electronic

components and the heat sink, the actual contact area is only 10%. Therefore, an flexible material with high thermal conductivity is required to fill the gap to remove the air with low thermal conductivity and establish an effective heat conduction channel, speeding up the heat dissipation of electronic components[33-34]. The present ordered GFs/NBR composites have high flexibility, high elasticity, high thermal conductivity and heat transfer rate for potential applications in heat dissipation of electronic components. As shown in Fig.7A, the heat dissipation performance of the 3D printing composites with different ordered orientation of GFs was evaluated for application in the substrate of LED light. In the initial stage, all LED lights showed a similar surface temperature of ca.38.6℃. However, as the working time increases, the surface temperature of the LED lamp with a GFs/NBR substrate is lower than that of the single LED lamp. The equilibrium temperature of the LED lights was about 53.6ºC, 54.3ºC, 55.6ºC and 61.7ºC for containing with GFs/NBR substrate with ordered GFs orientation (90º, 45º and 0º) and a blank substrate, respectively. This result proves the excellent heat dissipation performance of the 3D printing composite with 90º ordered GFs orientation. We then applied these 3D printing composites to the computer central processing unit to further evaluate their heat dissipation performance as shown in Fig.7B. When the nine capacitors reached steady state, the surface temperature is *ca.* 47.3ºC. After being covered with a heat dissipation box made of the 3D printing composite, the surface temperature dropped to 43.2ºC. These results indicate that the present composite with ordered orientation of GFs can effectively transfer the heat for the heat dissipation of electronic components.

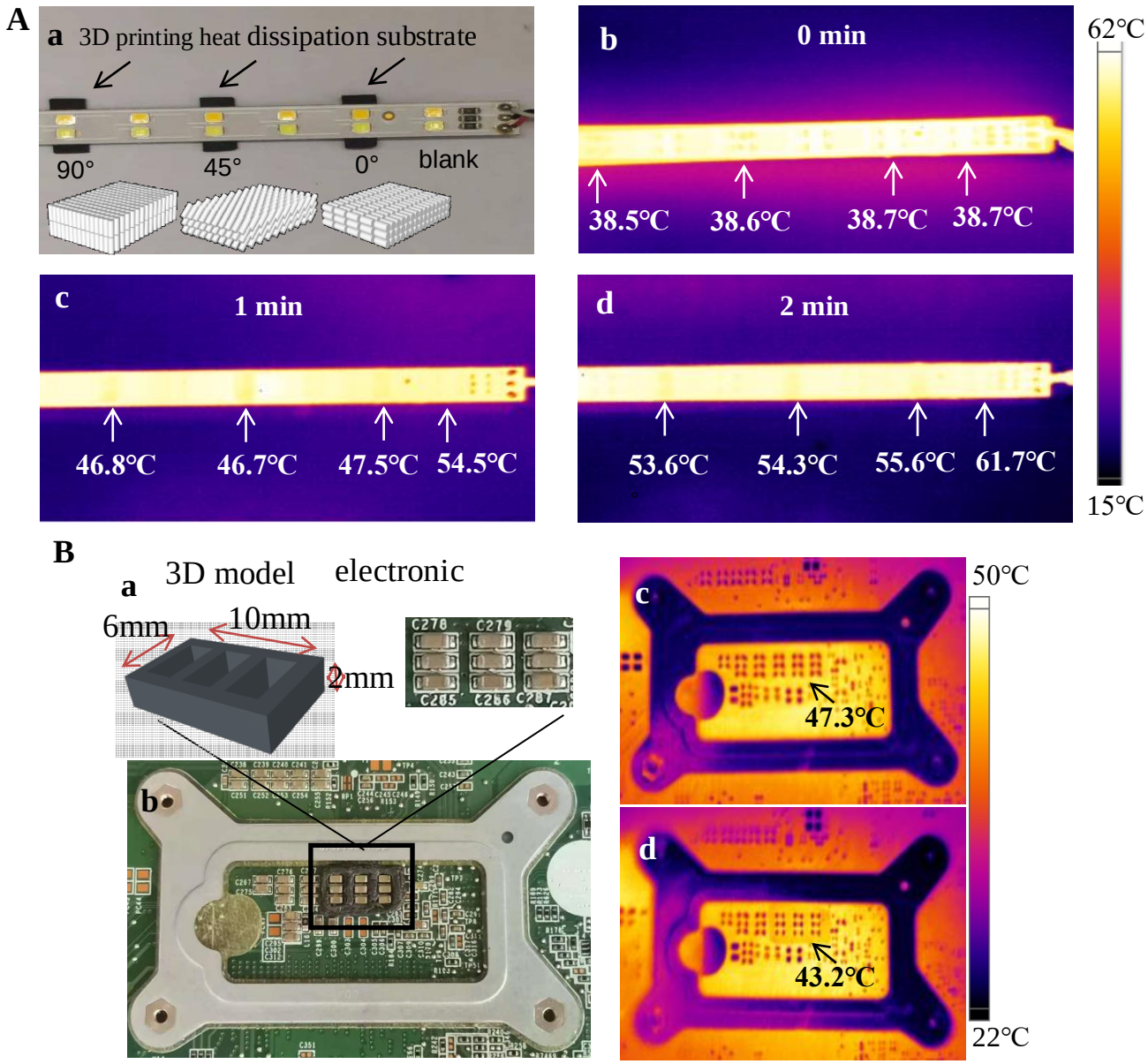

Fig.7. (A) (a) Optical of a LED strip with 3D printing composite substrate, the thermal images of a LED strip with 3D printing composite substrate as function of working time, (b) 0, (c) 1.0min and (d) 2.0min. (B) (a-b) Optical of a computer central processing unit fixed on the customized 3D thermal dissipation substrates, the thermal images of a computer central processing unit (c) without and (d) with fixed on the customized 3D thermal dissipation substrates.

4. Conclusion

In this study, we developed a novel hybrid ink composed of thermally conductive GFs and NBR matrix. Through the efficient and robust DIW 3D printing process, flexible, thermally conductive while electrically insulating 3D structures

were successfully prepared, in which controlled alignment and orientation of GFs was also achieved by tuning the printing direction of the nozzle. The thermal conductivity of the 3D printing composite with 90° oriented GFs increased from 0.4 to 1.2 W m^{-1} K^{-1}, which was close to the thermal conductivity of single GFs (1.4 W m^{-1} K^{-1}). At the same time, the 3D printing composites also exhibit good flexibility and elastic properties. Equipped with the customized composite substrates, the heat dissipation performance of LED lights and computer CPU has also been greatly improved due to the orderly orientation of thermally conductive fillers. The work confirms the formation of shear-induced alignment in 3D-printed nitrile rubber-reinforced glass fiber composites for various applications.

Acknowledgements

The authors are grateful for the support of the National Natural Science Foundation of China under grants (51773184 and U1810114), Shanxi Provincial Natural Science Foundation of China (201803D421081 and 20181102014).

Conflict of interest

The authors declared that they have no conflicts of interest to this work.

References

[1]Ma Meng, Xu Lin, Qiao Lele, Chen Si, Shi Yanqin, He Huiwen, Wang Xu, Nanofibrillated Cellulose/MgO@rGO composite films with highly anisotropic thermal conductivity and electrical insulation. *Chemical Engineering Journal* 392,123714 **(2020)**.

[2]Song Houfu, Liu Jiaman, Liu Bilu, Wu Junqiao, Cheng HuiMing, Kang Feiyu, Two-Dimensional Materials for Thermal Management Applications. *Joule* 2, 442-463 **(2018)**.

[3]Mehra Nitin, Mu Liwen, Ji Tuo, Yang Xutong, Kong Jie, Gu Junwei, Zhu Jiahua, Thermal transport in polymeric materials and across composite interfaces. *Applied Materials Today* 12, 92-130 **(2018)**.

[4]Li Jingchao, Zhao Xiuying, Wu Wenjie, Zhang Zhaoxu, Xian Yue, Lin Yutao, Lu Yonglai, Zhang Liqun, Advanced flexible rGO-BN natural rubber films with high thermal conductivity for improved thermal management capability. *Carbon* 162, 46-55 **(2020)**.

[5]Kusunose Takafumi, Uno Yoshinori, Tanaka Yuki, Sekino Tohru, Isotropic enhancement of the thermal conductivity of polymer composites by dispersion of equiaxed polyhedral boron nitride fillers. *Composites Science And Technology* 208,108770 **(2021)**.

[6]Wang Qingping, Bowen Chris R, Lei Wen, Zhang Haibo, Xie Bing, Qiu Shiyong, Li MingYu, Jiang Shenglin, Improved heat transfer for pyroelectric energy harvesting applications using a thermal conductive network of aluminum nitride in PMN-PMS-PZT ceramics. *Journal Of Materials Chemistry A* 6, 5040-5051 **(2018)**.

[7]Feng Yuezhan, Hu Ji, Xue Yang, He Chengen, Zhou Xingping, Xie Xiaolin, Ye Yunsheng, Mai Yiu-Wing, Simultaneous improvement in the flame resistance and thermal conductivity of epoxy/Al_2O_3 composites by incorporating polymeric flame retardant-functionalized graphene. *Journal Of Materials Chemistry A* 5, 13544-13556 **(2017)**.

[8]Wang Jun, Chen Yunsheng , Feng Yajie, Zhao Gang, Jian Xigao, Huang Qing, Yang Lingwei, Xu Jian, Influence of porosity on anisotropic thermal conductivity of SiC fiber reinforced SiC matrix composite: A microscopic modeling study. *Ceramics International* 46, 28693-28700 **(2020)**.

[9]Tang Lin, He Mukun, Na Xinyu, Guan Xiaofang, Zhang Ruihan, Zhang Junliang, Gu Junwei, Functionalized glass fibers cloth/spherical BN fillers/epoxy laminated composites with excellent thermal conductivities and electrical insulation properties. *Composites Communications* 16, 5-10 **(2019**).

[10]Liu Yingchun, Lu Maoping, Wu Kun, Yao Sa, Du Xiangxiang, Chen Guokang, Zhang Qian, Liang Liyan, Lu Mangeng, Anisotropic thermal conductivity and electromagnetic interference shielding of epoxy nanocomposites based on magnetic driving reduced graphene oxide@Fe3O4. *Composites Science And Technology* 174, 1-10 **(2019)**.

[11]Wang Mengjie, Liao Meizhen, Li Linhong, Li Maohua, Chen Yapeng, Hou Xiao, Yan Chao, Jiang Nan, Yu Jinhong, Graphdiyne for significant thermal conductivity enhancement at ultralow mass fraction in polymer composites. *2d Materials* 7,035007 **(2020)**.

[12]Yang Liu, Zhang Ling, Li Chunzhong, Bridging boron nitride nanosheets with oriented carbon nanotubes by electrospinning for the fabrication of thermal conductivity enhanced flexible nanocomposites. *Composites Science And Technology* 200,108429 **(2020)**.

[13]Cao Liu, Zhang Dong, Application potential of graphene aerogel in paraffin phase change composites: Experimental study and guidance based on numerical simulation. *Solar Energy Materials And Solar Cells* 223,110949 **(2021)**.

[14]Zhang Muxing, Wang Changling, Luo Ailian, Liu Zhenghao, Zhang Xiaosong, Molecular dynamics simulation on thermophysics of paraffin/EVA/graphene nanocomposites as phase change materials. *Applied Thermal Engineering* 166, 114639 **(2020)**.

[15]Bin Hoque Md Shafkat, Koh Yee Rui, Braun Jeffrey L, Mamun Abdullah, Liu Zeyu, Huynh Kenny, Liao Michael E, Hussain Kamal, Cheng Zhe, Hoglund Eric R, Olson David H, Tomko John A, Aryana Kiumars, Galib Roisul, Gaskins John T, Elahi Mirza Mohammad Mahbube, Leseman Zayd C, Howe James M, Luo Tengfei, Graham Samuel, Goorsky Mark S, Khan Asif, Hopkins Patrick E, High In-Plane Thermal Conductivity of Aluminum Nitride Thin Films. *Acs Nano* 15, 9588-9599 **(2021)**.

[16]Guo Haichang, Zhao Haoyuan, Niu Hongyu, Ren Yanjuan, Fang Haoming, Fang Xingxing, Lv Ruicong, Maqbool Muhammad, Bai Shulin, Highly Thermally Conductive 3D Printed Graphene Filled Polymer Composites for Scalable Thermal Management Applications. *Acs Nano* 15, 6917-6928 **(2021)**.

[17] Philipp Alexandra, Hummel Patrick, Schilling Theresa, Feicht Patrick, Rosenfeldt Sabine, Ertl Michael, Schoettle Marius, Lechner Anna M, Xu Zhen, Gao Chao, Breu Josef, Retsch Markus, Anisotropic Thermal Transport in Spray-Coated Single-Phase Two-Dimensional Materials: Synthetic Clay Versus Graphene Oxide. *Acs Applied Materials & Interfaces* 12, 18785-18791 **(2020)**.

[18]Wei Zhilei, Xie Wenqi, Ge Bangzhi, Zhang Zhejian, Yang Wanli, Xia Hongyan, Wang Bo, Jin Haiyun, Gao Naikui, Shi Zhongqi, Enhanced thermal conductivity of

epoxy composites by constructing aluminum nitride honeycomb reinforcements. *Composites Science And Technology* 199, 108304 **(2020)**.

[19]Zhuang Yuan, Song Wentong, Ning Gang, Sun Xueyan, Sun Zhongzheng, Xu Guowei, Zhang Bo, Chen Yening, Tao Shengyang, 3D-printing of materials with anisotropic heat distribution using conductive polylactic acid composites. *Materials & Design* 126, 135-140 **(2017**).

[20]Karl Niendorf, Bart Raeymaekers, Additive Manufacturing of Polymer Matrix Composite Materials with Aligned or Organized Filler Material: A Review. *Adv. Eng. Mater* 23, 2001002(**2021**).

[21]Wan Xue, Luo Lan, Liu Yanju, Leng Jinsong, Direct Ink Writing Based 4D Printing of Materials and Their Applications. *Advanced Science* 7, 2001000 **(2020)**.

[22]Rachel R. Collinoa, Tyler R. Ray, Rachel C. Fleming, James D. Cornell, Brett G. Compton, Matthew R. Begley, Deposition of ordered two-phase materials using microfluidic print nozzles with acoustic focusing. *Extreme Mechanics Letters* 8 96-106 (**2016**).

[23]Paul Wadsworth, Isaac Nelson, Debora Lyn Porter, Bart Raeymaekers, Steven E. Naleway, Manufacturing bioinspired flexible materials using ultrasound directed self-assembly and 3D printing. Materials & Design 185, 108243 (**2020**).

[24]Brett G. Compton, Jennifer A. Lewis, 3D-Printing of Lightweight Cellular Composites. *Adv. Mater* 26, 5930–5935(**2014**).

[25]A. Sydney Gladman, Elisabetta A. Matsumoto, Ralph G. Nuzzo, L. Mahadevan, Jennifer A. Lewis, Biomimetic 4D printing. *Nature Materials* 15, 413(**2016**).

[26]James P. Lewicki, Jennifer N. Rodriguez, Cheng Zhu, MarcusA.Worsley, Amanda S.Wu, Yuliya Kanarska, John D. Horn, Eric B. Duoss, Jason M. Ortega, William Elmer, Ryan Hensleigh, RyanA. Fellini & Michael J. King, 3D-Printing of Meso-structurally Ordered Carbon Fiber/Polymer Composites with Unprecedented Orthotropic Physical Properties. *Scientific Reports* 7, 43401(**2017**).

[27]Ma Guowei, Li Zhijian, Wang Li, Wang Fang, Sanjayan Jay, Mechanical anisotropy of aligned fiber reinforced composite for extrusion-based 3D printing. *Construction And Building Materials* 202, 770-783 **(2019)**.

[28]Wang Ridong, Zobeiri Hamidreza, Lin Huan, Qu Wangda, Bai Xianglan, Deng Cheng, Wang Xinwei, Anisotropic thermal conductivities and structure in lignin-based microscale carbon fibers. *Carbon* 147, 58-69 **(2019)**.

[29]Yiotis Andreas G, Kainourgiakis Michael E, Charalambopoulou Georgia C, Stubos Athanassios K, Microscale characterisation of stochastically reconstructed carbon fiber-based Gas Diffusion Layers; effects of anisotropy and resin content. *Journal Of Power Sources* 320, 153-167 **(2016)**.

[30]Lin Shangchao, Cai Zhuangli, Wang Yang, Zhao Lingling, Zhai Chenxi, Tailored morphology and highly enhanced phonon transport in polymer fibers: a multiscale computational framework. *Npj Computational Materials* 5, 126 **(2019)**.

[31]Zhang Rubing, Hou Xianbo, Ye Changshou, Wang Baolin, Fang Daining, Fabrication and properties of fibrous porous mullite-zirconia fiber networks with a quasi-layered structure. *Journal Of the European Ceramic Society* 36, 3539-3544 **(2016)**.

[32]Priyadarsini Morampudi, Kiran Kumar Namala, Yeshwanth Kumar Gajjela, Majjiga Barath, Ganaparthy Prudhvi, Review on glass fiber reinforced polymer composites. *Materials Today: Proceedings* 43, 314-319(**2021**).

[33]Ha Taeyong, Kim DongGyun, Ka JaeWon, Kim YongSeok, Koh WonGun, Lim Ho Sun, Yoo Youngjae, Simultaneous effects of silver-decorated graphite nanoplatelets and anisotropic alignments on improving thermal conductivity of stretchable poly(vinyl alcohol) composite films. *Composites Part a-Applied Science And Manufacturing* 138, 106045 **(2020)**.

[34]Zhuang Yafang, Zheng Kun, Cao Xinyu, Fan Qingrui, Ye Gang, Lu Jiaxin, Zhang Jingnan, Ma Yongmei, Flexible Graphene Nanocomposites with Simultaneous Highly Anisotropic Thermal and Electrical Conductivities Prepared by Engineered Graphene with Flat Morphology. *Acs Nano* 14, 11733-11742 **(2020)**.